Spectral Monitoring Techniques for Optically Deep Mine Waters

Brandon K. Holzbauer-Schweitzer[1], Robert W. Nairn[2]

[1]*Graduate Research Assistant, University of Oklahoma, 202 West Boyd Street, Norman, Oklahoma, 73019, Bholzbauersch10@ou.edu*

[2]*Professor, University of Oklahoma, 202 West Boyd Street Room 334, Norman, Oklahoma, 73019, Nairn@ou.edu, ORCID 0000-0003-1400-6289*

Abstract

Remote estimation of water quality is of increasing interest to monitoring professionals. Unfortunately, environmental and technical limitations inhibit widespread application. The purpose of this study was to demonstrate spectral monitoring techniques utilizing data from two different platforms. Results describe strong linear relationships between remotely collected multispectral reflectance and in-situ metal concentrations. Spatial regression techniques produced a model capable of predicting particulate iron concentrations with moderate confidence (R^2_{adj} = 0.83) and reasonable error (SSR = 69.80). Overall, remote environmental monitoring represents a novel tool to advance and improve the effectiveness of traditional monitoring efforts.

Keywords: Geographically weighted regression, optical depth, water quality, unmanned aerial system

Introduction

As electromagnetic energy reaches an object several interactions will occur (e.g. reflection, transmission, absorption, and scattering) between photons and particles within the media (e.g. optically active constituents (OACs)) until either photons are reemitted (e.g. reflected), or all energy is consumed (e.g. absorbed). In cases where the water column is transparent (e.g. low concentrations of OACs), photons interact with the bottom substrate altering the expected energy signal (e.g. optically shallow water (OSW)). Conversely, if OACs are present in elevated concentrations, even within physically shallow surface waters, and the bottom substrate is not visible, observable energy will decay at an exponential rate and interactions with the substrate will be minimal (e.g. optically deep water (ODW)) (Zeng et al. 2017). Traditional determinations of optical depth (OD) utilize the Beer-Lambert Law and require the measurement or calculation of the spectral intensity of incoming solar radiance (I), the spectral intensity of emitted (e.g. reflected or scattered) solar radiance (I_O), absorption coefficient (κ) of the object, density (ρ) of the object, and the solar zenith angle (Θ) of I. Application of this methodology has been based primarily in meteorological sciences, typically to estimate the OD of water vapor and other aerosols in Earth's atmosphere (Filonchyk et al. 2019).

Small Unmanned Aerial Systems (sUAS) have demonstrated effectiveness in performing remote sensing of traditional OACs (e.g. chlorophyll-a) in ODWs (e.g. Su 2017). Literature gaps exist in the application of these technologies in OSWs and their use for the examination of mine drainage. Therefore, the purpose of this study was two-fold: to examine the feasibility of utilizing sUAS-derived multispectral (MS) imagery (e.g. tens of spectral measurements) to estimate in-situ metal concentrations in ODWs and to investigate in-situ OD utilizing spectroradiometer-derived hyperspectral (HS) data (e.g. thousands of spectral measurements) to discern the effect that remotely sensing substrate has on sUAS-derived MS imagery.

Methods

Study Site Description

Spectral data were collected from the surface of an oxidative process unit (Cell one (C1)),

a part of the larger Mayer Ranch Passive Treatment System (MRPTS) in May, June, and July of 2019. MRPTS is located within the Tar Creek watershed and Tar Creek Superfund Site, and the Oklahoma portion of the Tri-State Mining District (TSMD) (fig. 1). This ten-cell PTS, operated with two parallel treatment trains, was designed to promote various natural biogeochemical processes in specific process units. Overall, the PTS has effectively treated artesian net-alkaline ferruginous lead-zinc mine drainage since late 2008 (Nairn et al. 2009).

Spectral Instrument Calibration and Operation

Before data collection, each instrument was calibrated correctly. The Analytical Spectral Devices (ASD) FieldSpec3 was optimized and standardized with a white calibrated reflectance panel (CFP) designed to reflect 95 – 99% of electromagnetic energy. During this process, the instrument measured reflected electromagnetic energy from the CFP to establish a baseline reference of approximately 100%. To calibrate the MicaSense RedEdge sensor on the sUAS, an image of the same CFP was taken pre- and post-flight. The image processing software (Pix4DMapper) used the two calibration images to account for changes in solar conditions throughout the flight and to transform the uncompressed 16-bit, 1,280 by 960-pixel, digital number values into spectral reflectance values.

In May, the ASD FieldSpec3 was used to collect HS (e.g. 350 – 2500 nm) profiles from a pair of catwalks located in C1. Measurements were collected nadir to the water surface, approximately one m above the surface at one m horizontal increments starting at the water's edge (0 m) to the end of the catwalks (4 and 6 m for the northeast and southeast catwalks, respectively). At each location, the spectral profile measured was an average of five sets of ten measurements, taken in 0.1 s increments. Raw data files were post-processed to spectral reflectance with the ASD ViewSpec Pro software.

In June and July, the Aerial Technology International (ATI) AgBot equipped with

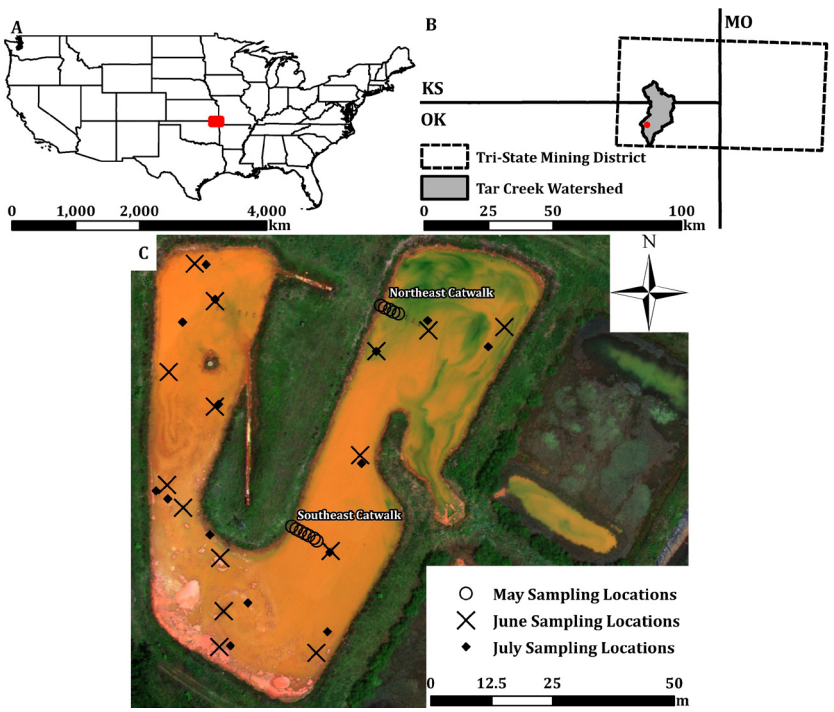

Figure 1 *Location of (A) TSMD in the central United States, (B) Tar Creek watershed in Oklahoma and Kansas, and (C) C1 within MRPTS with May catwalk and June and July in-pond sampling locations identified.*

the RedEdge sensor was used to collect MS reflectance imagery within ±2 h of local solar noon. This vertical take-off and landing (VTOL) quadcopter sUAS measures MS reflectance in five discrete spectral bands (e.g. blue, green, red, red edge (RE), and near-infrared (NIR)) simultaneously with center points at 475, 560, 668, 717, and 840 nm, respectively. Each sUAS flight was completed autonomously, with missions developed in Mission Planner software V.1.3.37. Missions covered approximately 81,000 m^2, at speeds of 6 m s^{-1}, an altitude of 50 m above ground level, with 75% image side and overlap to ensure accurate georeferencing, mosaicking, and high-quality data. Using these mission parameters produced a spatial resolution of roughly 6.82 cm $pixel^{-1}$.

In-situ Surface Water Quality Sampling

Fifteen in-situ surface water grab samples were geo-located and collected from C1 within a one h window of each sUAS flight completion. To adequately address the spatial distribution of surface water quality, ten sampling locations were established around the water's edge of C1. An additional five samples were collected throughout the center of C1 via canoe (fig. 1). Water's edge samples were collected from C1 with a fully extended swing-arm sampling pole (approximately 3.6 m in length). All samples were collected approximately 0.5 m below the water surface, or at the point the 1-L HDPE sample bottle was no longer visible. Samples for analyses of total and dissolved (0.45-mm) metal concentrations were collected at each location following EPA approved methods.

Assessing the Effects of Optical Depth

After the collection of HS data, Secchi disk depth (SDD) and actual physical depth (AD) were measured at the same one m horizontal increments. To minimize the resuspension of substrate and modification to the water column's optical properties, SDD was measured first. Then AD was measured by lowering a weighted line into the water column until it contacted the surface of the substrate. With the assumption that SDD ~ OD, and when the ratio between SDD and AD was equal to one, interferences from the substrate were expected. To characterize this phenomenon in terms of sUAS-derived MS imagery, an exponential relationship was developed. This relationship used HS reflectance data extracted with respect to the red band (668 nm) of the RedEdge sensor and the SDD AD ratio. Visualization of the extent of interference from OSWs (e.g. SDD:AD > 1) was completed utilizing the Raster Calculator, the statistically derived exponential relationship, and the sUAS-measured red band reflectance in ArcMap 10.6.1.

Results and Discussion

Estimating In-situ Surface Water Quality

In pond metal concentrations were typical of net alkaline metal-rich mine waters (tab. 1). Although MS interferences from wind action (e.g. glint) and cloud cover were minimal, interferences occurred from surface scum (e.g. amorphous iron-oxyhydroxide) and algae (e.g. chlorophyll-a), particularly in the southwestern and northeastern portions of C1, respectively. If these conditions affected either dataset, outliers were identified and removed utilizing the inter-quartile range.

In-situ water quality and MS reflectance were defined as the dependent and independent variables, respectively. In reality, OACs (e.g. metals) are independent of and effect the MS signals measured. To that end, Ca, Co, K, Li, Mg, Mn, Na, Ni, Pb, S, Si, and Zn exhibited strong collinearity ($R > 0.90$) and except for Si and Zn exhibited moderately strong inverse relationships ($R < -0.65$) with the untransformed green band (tab. 1). Furthermore, Cd and Fe also displayed collinearity ($R = 0.84$) and exhibited the most robust relationships ($R > 0.80$) with the log-transformed and untransformed red band, respectively. Surprisingly, Zn was not correlated with Cd ($R = 0.23$), and the strongest relationship observed was with the green and RE ratio ($R = -0.68$). Al and Cu were not collinearly related with any other metal and required log transformations to develop any meaningful relationship ($R = -0.50$ and -0.75, respectively). Overall, the optical fraction (e.g. total and particulate) of metal concentrations were more strongly correlated then the non-optical fraction (e.g. dissolved).

For some metals (e.g. Cd, Pb, and Zn), the

prominence and adsorption capabilities of iron-oxyhydroxides were likely contributing to the observed relationships. Additionally, the inverse relationships with the green band were the result of fundamental electromagnetic interactions. Locations with higher metal (e.g. Fe) concentrations reflected more red energy and absorbed more green energy. Conversely, as concentrations of the predominant OAC (e.g. Fe) decreased, the amount of red energy reflected also decreased, while reflected green energy increased.

A series of surface water quality maps were generated in ArcMap 10.6.1 (fig. 2) using these data. The red band was the input to a geographically weighted regression (GWR) model, and local polynomial interpolation (LPI) was used to extrapolate particulate Fe concentrations across C1 (fig. 2A). These maps have a spatial resolution (approximately 30 cm pixel^{-1}) more representative of in-situ water quality than traditional monitoring efforts (e.g. single concentration applied to an entire water body), including a spatial component to the regression model substantially improved performance. Overall, the GWR model produced a sum of squared residuals (SSR), sigma, Akaike information criterion (AICc), and an adjusted R^2 of 69.80, 2.11, 112.09, and 0.83, respectively (fig. 2B). The relatively high SSR is due to an absence of sampling locations in the northern portion of C1 (fig. 2C). At this location (e.g. *hot spot*), there were not sufficient neighbours to develop meaningful statistical relationships, resulting in arbitrarily high residuals to be interpolated.

Table 1 *Summary statistics (n = 23) for sUAS-derived MS reflectance (decimal percent) and in-situ total metal concentration data (mg L^{-1} unless otherwise noted) with the strongest relationship (R), MS band (X), any transformations (Trans.), and the metals fraction (D = dissolved, P = particulate, T = total) exhibiting R; * = $\mu g\ L^{-1}$.*

Parameter	Mean	Maximum	Minimum	R	X	Trans.	Fraction
MS Reflectance							
Blue	0.04 ± 0.01	0.08	0.03	-	-	-	-
Green	0.11 ± 0.01	0.13	0.08	-	-	-	-
Red	0.20 ± 0.03	0.26	0.18	-	-	-	-
NIR	0.13 ± 0.05	0.30	0.08	-	-	-	-
RE	0.20 ± 0.04	0.32	0.15	-	-	-	-
[Total Metals]							
Al	0.06 ± 0.05	0.28	0.02	-0.50	Green	Log10	P
Ca	681.43 ± 59.93	753.96	616.68	-0.68	Green	-	T
Cd*	1.87 ± 0.68	3.00	1.00	0.83	Red	Log10	P
Co	0.04 ± 0.004	0.05	0.04	-0.68	Green	-	T
Cu*	4.13 ± 1.30	8.00	2.00	-0.75	Blue	Log10	P
Fe	11.14 ± 5.90	29.15	5.20	0.88	Red	-	P
K	22.41 ± 2.41	25.08	19.72	-0.71	Green	-	T
Li	0.26 ± 0.03	0.29	0.23	-0.70	Green	-	T
Mg	154.46 ± 14.29	171.36	139.12	-0.69	Green	-	T
Mn	1.17 ± 0.10	1.29	1.05	-0.65	Green	-	T
Na	99.02 ± 9.22	109.45	88.82	-0.71	Green	-	T
Ni	0.66 ± 0.06	0.74	0.58	-0.67	Green	-	T
Pb	0.30 ± 0.03	0.33	0.26	-0.75	Green	-	T
S	746.29 ± 73.42	831.56	660.99	-0.69	Green	-	T
Si	6.84 ± 0.60	7.60	6.04	0.75	Red	-	P
Zn	4.11 ± 0.37	4.58	3.56	-0.68	Green:RE	-	T

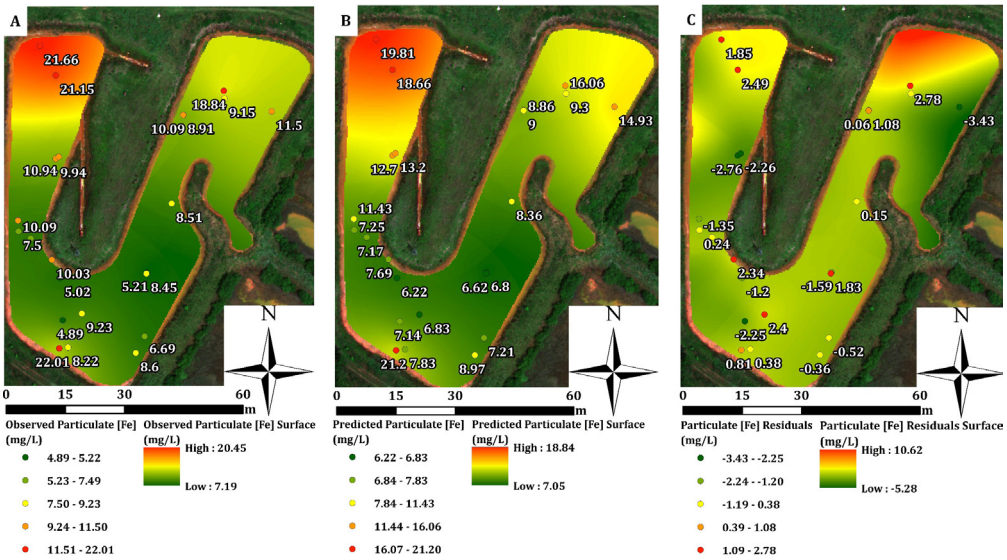

Figure 2 Observed (A) and GWR predicted (B) spatial water quality maps with resulting residuals (C); point values are labeled and were extrapolated with LPI.

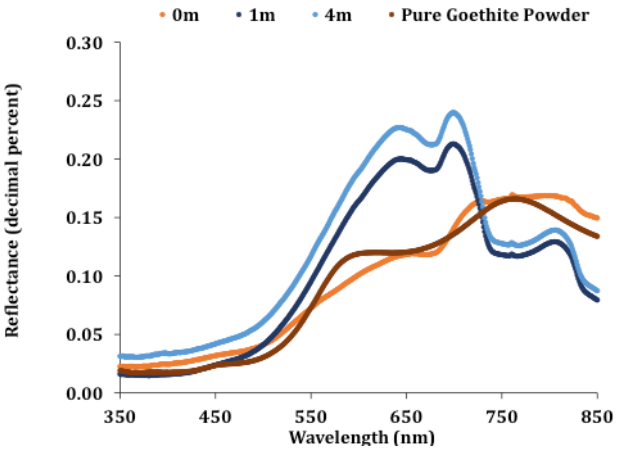

Figure 3 HS profiles collected at the northeastern catwalk in May 2019 (Goethite data: Kokaly et al. 2017).

Determination of Optical Depth Influence

The assumption that SDD ~ OD was verified by examining the shape and magnitude of spectral profiles collected when the substrate was and was not visible through the water column at increasing distances and depths from the water's edge (0 m) (fig. 3). Remotely sensing bottom substrates not only decreased the overall energy reflected (by approximately 20%) but modified the shape of the spectra (e.g. changes to peak reflectance wavelengths) (fig. 3). Furthermore, when the substrate was visible through the water column, a moderately strong negative exponential relationship existed that was representative of the exponential decay of spectral energy in water (R = 0.75). A spatial map identifying the extent of interference caused by OSW (e.g. SDD:AD > 1) within C1 was developed (fig. 4). Based on these results, it would be expected to measure interference from the substrate in the northeast portion of C1. Unfortunately, this identification of OSW was caused by remotely sensed algae (fig. 1), rather than the substrate, resulting in lower red, relative to green, MS reflectance. Overall,

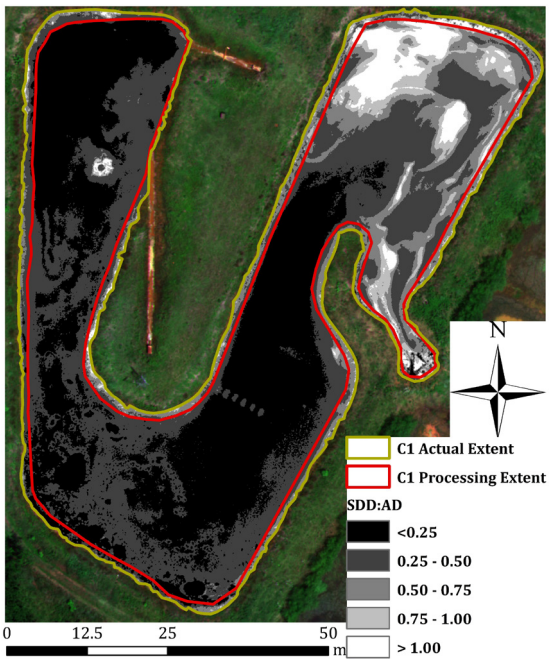

Figure 4 *Extent of expected OD interferences (e.g. SDD:AD > 1) within C1.*

these results represent a valid method of identifying the extent of OD interference to evaluate the feasibility of performing remote surface water quality monitoring in optically complex surface waters.

Conclusions and Future Work

Although the developed spatial water quality model exhibits relatively low residuals, these results have not been validated. It is also likely the results are site and mine drainage (e.g. net alkaline ferruginous lead-zinc waters) specific. Furthermore, the *success* of the model was primarily driven by the dominant optical properties of C1 (e.g. substantial presence of iron-oxyhydroxides) and is untested in the transparent artesian source waters. Rapid identification and estimation of OD in any type of water can address the feasibility of utilizing sUAS technologies for environmental monitoring. Results of the OD analysis support decreasing processing extents (e.g. excluding edge effects) to minimize interferences from OSWs and verified much of the studied water body (e.g. C1) were ODWs, suggesting the presented spatial water quality model was valid and representative of in-situ surface water conditions. Future efforts should include continued training and validation of the developed models in mine waters characteristic of the TSMD. Additional training and validation must occur outside the TSMD in waters affected by other sources of mine drainage (e.g. net acidic coal mine drainage) to address site-specificity. As sUAS technologies and spatial water quality models improve remote monitoring, they can contribute substantial quantities of environmental data (e.g. identify *hot spots* to focus traditional monitoring efforts), decrease field and laboratory costs, and increase spatial and temporal resolutions of traditional monitoring efforts.

Acknowledgments

This work was supported by the Grand River Dam Authority (Agreements GRDA 060910 and GRDA 08272015). The authors thank members of the Center for Restoration of Ecosystems and Watersheds (CREW), Earth Observation and Modeling Facility (EOMF), and private landowners for assistance in data collection, providing additional spectral instrumentation, and access to private lands, respectively.

References

Davis JA, Leckie JO (1978) Surface ionization and complexation at the oxide/water interface II. Surface properties of amorphous iron oxyhydroxide and adsorption of metal ions. J Colloid and Interface Science 67:90-107, doi:10.1016/0021-9797(78)90217-5.

Filonchyk M, Yan H, Zhang Z, Yang S, Li W, Li Y (2019) Combined use of satellite and surface observations to study aerosol optical depth in different regions of China. J Sci Rep 9:6174, doi:10.1038/s41598-019-42466-6.

Kokaly RF, Clark RN, Swayze GA, Livo KE, Hoefen TM, Pearson NC, Wise RA, Benzel WM, Lowers HA, Driscoll RL, Klein AJ (2017) USGS spectral library version 7. USGS Data Series 1035:61, doi:10.3133/ds1035.

Nairn RW, Beisel T, Thomas RC, LaBar JA, Strevett KA, Fuller D, Strosnider WH, Andrews WJ, Bays J, Knox RC (2009) Challenges in design and construction of a large multi-cell passive treatment system for ferruginous lead-zinc mine waters. J American Society of Mining and Reclamation 871-892, doi:10.21000/JASMR09010871.

Su TC (2017) A study of matching pixel by pixel (MPP) algorithm to establish an empirical model of water quality mapping, as based on unmanned aerial vehicle (UAV) images. Int. J Applied Earth Observation and Geoinformation 58:213-224, doi:10.1016/j.jag.2017.02.011.

Zeng C, Richardson M, King D (2017) The impacts of environmental variables on water reflectance measured using lightweight unmanned aerial vehicle (UAV)-based spectrometer system. J Photogrammetry and Remote Sensing 130:217-230, doi:10.1016/j.isprsjprs.2017.06.004.